ELIMINATING A RUB-INDUCED STARTUP VIBRATION PROBLEM IN AN ETHYLENE DRIVE STEAM TURBINE

by

John C. Nicholas

President and Chief Engineer

Rotating Machinery Technology, Inc.

Wellsville, New York

Stephen L. Edney

Technical Specialist in System Dynamics

Rolls-Royce Corporation

Indianapolis, Indiana

Terryl Matthews

Senior Mechanical Engineering Associate

The Dow Chemical Company

Houston, Texas

and

Francisco J. Mourente Varela

Maintenance Engineer, Rotating Equipment Group

Dow Chemical Ibérica, S.A.

Tarragona, Spain

John C. Nicholas is part owner, President, and Chief Engineer of Rotating Machinery Technology, Inc., a company that repairs and services turbomachinery, and manufactures bearings and seals. He has worked in the turbomachinery industry for 24 years in the rotor and bearing dynamics areas, including five years at Ingersoll-Rand and five years as Supervisor of the Rotordynamics Group at the Steam Turbine Division of Dresser-Rand.

Dr. Nicholas is a member of ASME, STLE, and the Vibration Institute. He has authored over 35 technical papers concerning tilting pad bearing design, pressure dam bearings, rotordynamics, and support stiffness effects.

He received his B.S. degree from the University of Pittsburgh (Mechanical Engineering, 1968) and Ph.D. degree from the University of Virginia (1977) in rotor and bearing dynamics. Dr. Nicholas holds patents for a stabilized double pocket sleeve bearing design and a spray bar blocker design that lowers tilting pad journal bearing operating temperatures.

Stephen L. (Steve) Edney is Technical Specialist in System Dynamics at Rolls-Royce Corporation located in Indianapolis, Indiana. He has a total of 18 years of industrial experience, primarily working on the machinery dynamics of gas and steam turbines. Dr. Edney's career started in the United Kingdom with eight years at GEC-Alsthom, followed by nine years at the Steam Turbine Division of Dresser-Rand. His involvement in this paper began while he was still with Dresser-Rand.

Dr. Edney received his B.Sc. (1983) and Ph.D. (1990) degrees in Mechanical Engineering from the University of Nottingham, England. He is a member of ASME and the Vibration Institute, and an associate member of IMechE. He holds one US Patent, and has authored numerous reviewed technical papers covering the finite element modeling of shafts, the nonlinear response of rotor-bearing systems to shock excitation, turbulence in tilting pad journal bearings, and the rotordynamics design of turbomachinery.

Terryl Matthews is a Senior Mechanical Engineering Associate with The Dow Chemical Company, Design and Construction, Houston, Texas. His responsibilities since joining Dow (1973), include specifications, technical support, mechanical and performance testing, consulting, and field assistance in the area of rotating equipment for Dow Chemical worldwide.

Mr. Matthews holds a B.S. degree (Mechanical Engineering, 1972) from the University of Houston. He is a member of ASME, a member of the ASME International Gas Turbine Institute's Industrial and Cogeneration Committee, a member of the ASME B73 Chemical Standard Pump Committee, a member of the API Committee on Refinery Equipment, and is a registered Professional Engineer in the State of Texas.

ABSTRACT

A 16 megawatt ethylene drive steam turbine built in 1973 experienced rub related startup vibration problems for many years. The turbine would lock into a rub as it accelerated through the rotor's first critical speed causing high vibration and often damage to components.

Many possible causes of the rub were identified including casing distortion from bound keys, a steam leak at the horizontal joint flange, and a deteriorated foundation after many years of operation subjected to high vibration. Finally, the sensitivity of the rotor's first critical speed was a concern.

This paper describes how these problems were attacked in a concerted effort to eliminate the rub-induced vibration. The horizontal joint seal face was redesigned to address the steam leak; all sliding keys were removed, cleaned, and lubricated; the foundation repaired and regrouted; the original labyrinth seals replaced with retractable packing; and a squeeze film damper added to reduce the critical speed response sensitivity.

INTRODUCTION

A 16 megawatt ethylene drive steam turbine built in 1973 and operating at a maximum continuous speed of 8400 rpm experienced rub related startup vibration problems for many years. The turbine would lock into a rub as it accelerated through the rotor's first critical speed of 3800 rpm. The rub would often continue up to operating speed, causing high 1× vibration that often exceeded 4.0 mils peak-to-peak at the vibration probes. Corresponding casing velocity readings peaked up to 0.7 in/s zero-to-peak, which would be classified in the danger zone on a vibration nomograph.

Many possible causes of the rub were identified including casing distortion from bound lateral expansion keys, a steam leak at the casing horizontal joint flange in the high-pressure packing area, and a deteriorated foundation after many years of operation subjected to high vibration. Also reviewed were the response characteristics of the rotor-bearing system and, in particular, the unbalance sensitivity of the first critical speed.

In a concerted effort to eliminate the rub-induced vibration, several problem areas were addressed during a scheduled maintenance plant shutdown. In an attempt to eliminate the steam leak, the horizontal flange metal-to-metal contact area was decreased, increasing the contact loading. Furthermore, all sliding keys were removed, cleaned, and lubricated, and the foundation repaired and regrouted to improve structural rigidity that is essential for the proper control of rotor vibration (Nicholas, et al., 1986). In addition, for both startup and efficiency reasons, the original interstage labyrinth seals were replaced with retractable packing (Johns, et al., 1997). The tilting pad journal bearings were redesigned to provide optimum damping (Nicholas, 1994), and a squeeze film damper added to further reduce the critical speed response sensitivity (Edney and Nicholas, 1999). Lastly, the coupling was replaced with a reduced moment design to move a shaft overhang critical speed.

Comparing field vibration data for the turbine prior to the overhaul with data after the aforementioned modifications clearly shows that the rub-induced startup vibration has indeed been eliminated. The solution methodology presented herein is intended to be a template that offers practical guidance for resolving similar startup vibration problems often encountered in the rotating equipment industry.

DESCRIPTION OF PROBLEM

Figure 1 is a photo of the 16 megawatt ethylene drive steam turbine rotor. The steam or inlet end is on the left where the thrust collars are clearly visible along with the mechanical trip mechanism. The exhaust or coupling end on the right comprises a double flow opposed exhaust section, a side engaging turning gear, and a tapered hydraulic fit coupling shaft end with locking nut. The rotor weighs 5029 lb with a bearing span of 97.7 inches. The midspan shaft diameter is 13.0 inches.

The turbine, built and installed in 1973, operates between a minimum governor speed of 6500 rpm and maximum continuous speed of 8400 rpm. A typical startup is illustrated in Figure 2, in which the turbine's steam end horizontal displacement probe vibration increases to 120 microns peak-to-peak (4.7 mils peak-to-peak) at 3800 rpm. At 4200 rpm, the vibration suddenly drops to 30 microns peak-to-peak (1.2 mils peak-to-peak) and remains at that level as the turbine accelerates up to 6800 rpm. In this case, it appears that the rotor locked into a hard rub at low speed and then suddenly dropped out of the rub right after passing through the first critical speed.

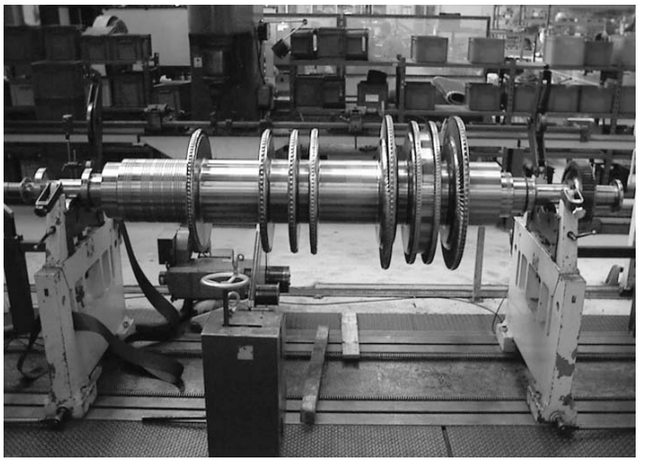

Figure 1. Integrally Forged Steam Turbine Rotor.

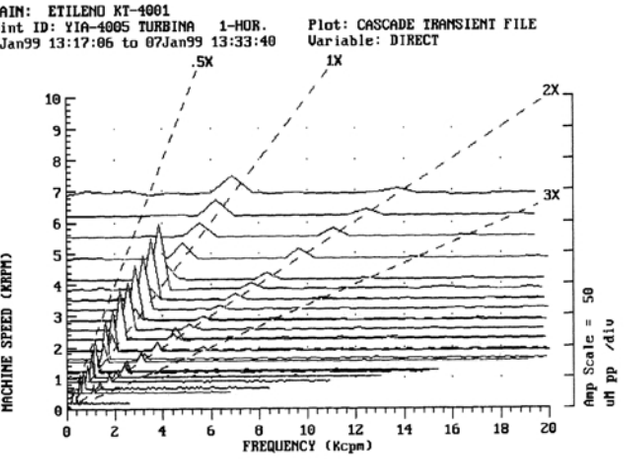

Figure 2. Steam End Horizontal Displacement Probe Vibration – 07Jan99.

In contrast, the exhaust end horizontal bearing case velocity probe's signal for the same startup is shown in Figure 3. The same increasing vibration trend up to the first critical speed at 3800 rpm is observed as in Figure 2. However, the case vibration remains high up to 6800 rpm reaching a peak of 8 mm/s zero-to-peak (0.3 in/s zero-to-peak). Unlike the displacement probe, the velocity probe appears to indicate that the turbine locked into a rub at low speed with the rub continuing up to operating speed.

A different startup is illustrated in Figure 4. In this case, the steam end horizontal displacement probe vibration increases up to 80 microns peak-to-peak (3.1 mils peak-to-peak) at 3800 rpm, decreases slightly after the critical speed, increasing again to 80 microns peak-to-peak at overspeed (9300 rpm). This trend suggests that the rotor locked into a rub as it traversed the first critical speed, with the rub continuing all the way up to overspeed.

Yet another startup taken from the steam end horizontal displacement probe is illustrated in Figure 5. In this case the vibration ramps up to 100 microns peak-to-peak (3.9 mils peak-to-peak) at 6500 rpm. The corresponding exhaust end bearing case horizontal velocity signal is depicted in Figure 6 showing a peak magnitude of 17 mm/s zero-to-peak (0.7 in/s zero-to-peak) at 6600 rpm. This value is in the danger zone and most probably indicates that the rotor locked into a very hard rub.

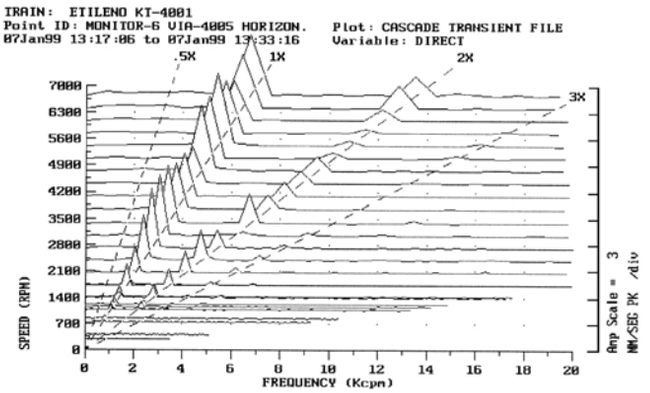

Figure 3. Exhaust End Horizontal Bearing Case Velocity Probe Vibration – 07Jan99.

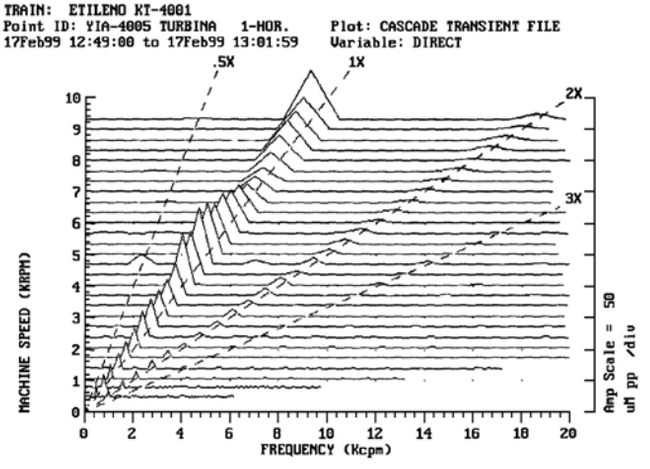

Figure 4. Steam End Horizontal Displacement Probe Vibration – 17Feb99.

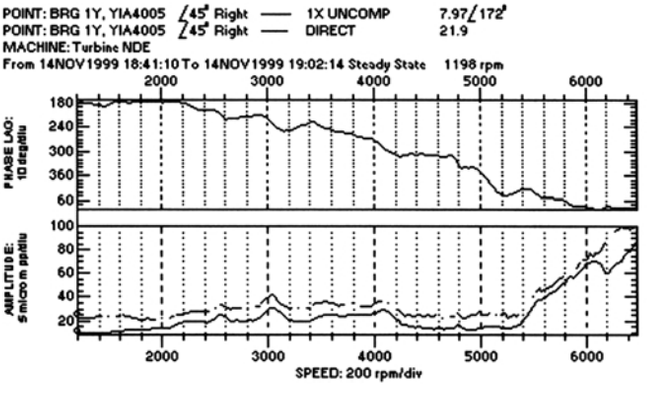

Figure 5. Steam End Horizontal Displacement Probe Vibration – 14Nov99.

Time histories of turbine vibration from February 1999 until May 1999 are illustrated in Figures 7 and 8. From Figure 7, the steam end horizontal displacement probe's normal vibration level is around 40 microns peak-to-peak (1.6 mils peak-to-peak) with peaks spiking up to 125 microns peak-to-peak (4.9 mils peak-to-peak). Casing readings for the exhaust end horizontal velocity probe are shown in Figure 8. Normal velocity levels between 4.0 and 8.0 mm/s zero-to-peak (0.16 and 0.32 in/s zero-to-peak) are evident with peaks spiking up to 20 mm/s zero-to-peak (0.8 in/s zero-to-peak).

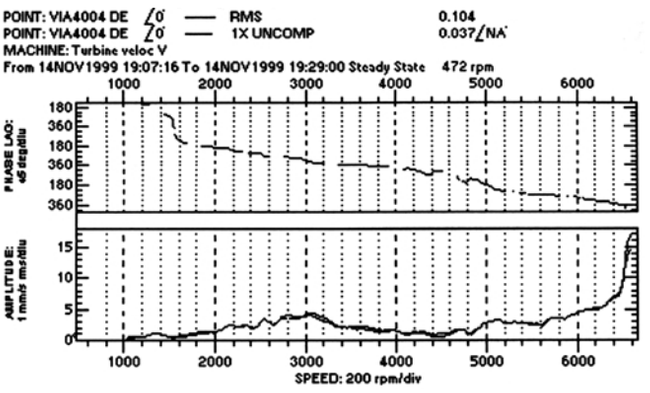

Figure 6. Exhaust End Horizontal Bearing Case Velocity Probe Vibration – 14Nov99.

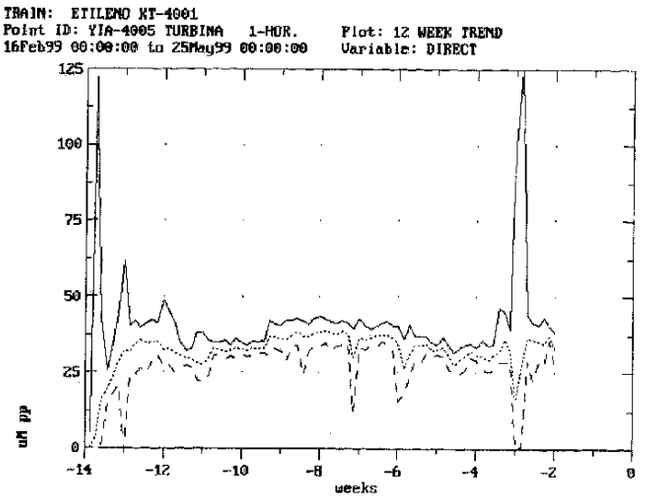

Figure 7. Time Trend of Steam End Horizontal Displacement Probe Vibration Before Overhaul.

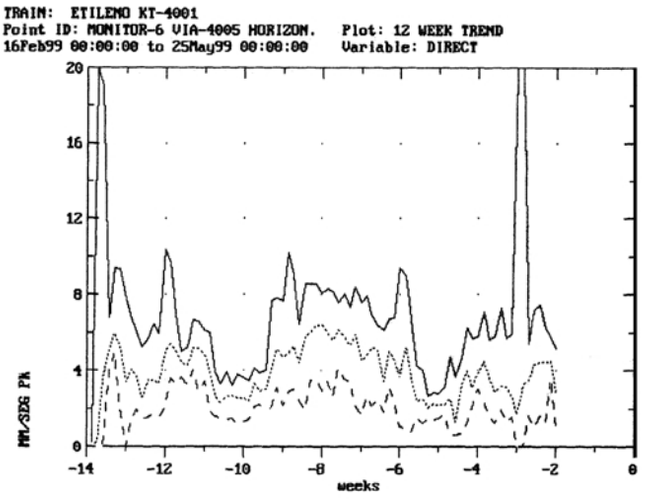

Figure 8. Time Trend of Exhaust End Horizontal Bearing Case Velocity Probe Vibration Before Overhaul.

Repeated exposure to vibration levels of this magnitude took its toll on the foundation, which deteriorated markedly over the years resulting in many cracks. In addition to the deteriorating foundation, the equipment also suffered abuse. Figure 9, for example, shows evidence of substantial rub marks on the rotor in the double

flow section, while Figure 10 shows severe labyrinth seal damage. Both these photographs are clearly indicative of a very serious rub problem, and are quite typical of the troubles that existed for many years.

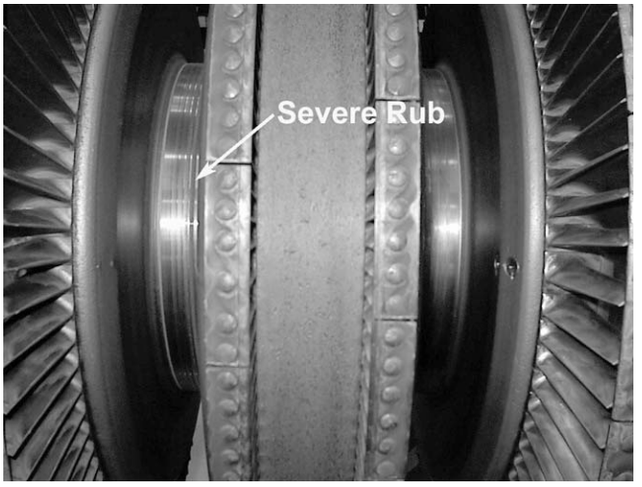

Figure 9. Shaft Rub Marks in Double Flow Section.

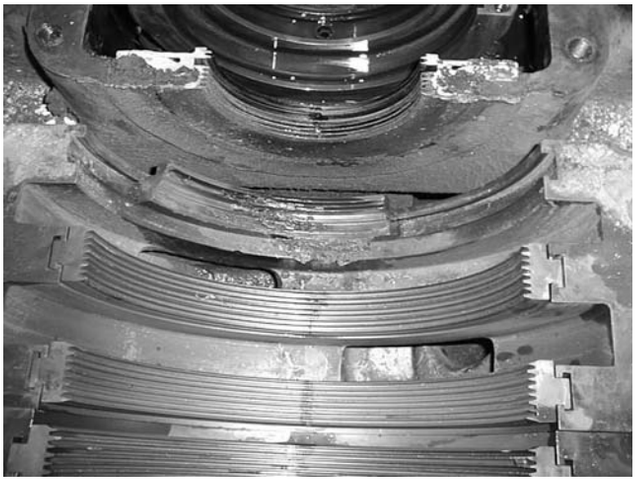

Figure 10. Damaged Labyrinth Seals.

STEAM TURBINE

A cross-sectional view of the steam turbine is shown in Figure 11. It is a condensing design with a double flow opposed exhaust section, and an exhaust end mounted side engaging turning gear. The rotor (Figure 1) is a solid forging with a L_b/D_s ratio of 7.5. In general, the flexural response of a rotor increases with L_b/D_s ratio, resulting in higher amplification factors and increased sensitivity to unbalance. A good rule of thumb is that a well-proportioned rotor should have a L_b/D_s ratio less than 10, as is the case here.

However, there are other factors and criteria that should be considered in the design of a well-balanced rotor-bearing-support system. These include the shaft proportions through the packing cases and overhangs (and hence stiffness distribution), the location and modal influence of any concentrated masses (such as wheels, thrust discs, and couplings), bearing design, and support structure characteristics. For example, a small shaft diameter through the packing case and journal, although good for reducing steam leakage and improving bearing performance, can significantly reduce the overall flexibility of the rotor resulting in an increase in response. A second and equally as important rule of thumb, therefore, is that the average direct bearing stiffness should be less

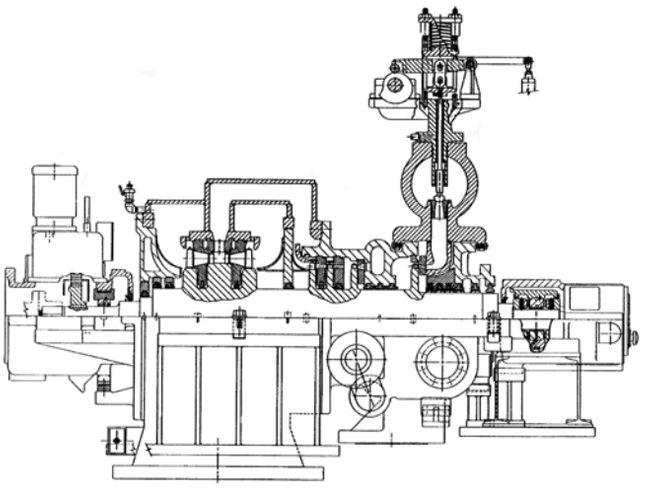

Figure 11. Cross Sectional View of Steam Turbine.

than half that of the rotor. By allowing rotor motion at the bearings, the available oil film damping is much more effective in suppressing shaft vibration.

Original Bearings and Coupling

The turbine was originally designed with spherically seated pressure dam sleeve bearings and a continuously lubricated gear type coupling. The steam end bearing was 4.5 inches in diameter by 3.125 inches long yielding a unit load of 152 psi, and the exhaust end bearing 4.5 inches in diameter by 3.5 inches long with a unit load of 184 psi. With this arrangement, the average direct stiffness of the bearings was roughly 1,900,000 lb/in, which is of a similar magnitude to the rotor's stiffness of 2,200,000 lb/in. These values clearly did not meet the stiffness flexibility ratio of a well-balanced rotordynamic system.

In addition, the effective overhung moment of the continuously lubricated gear coupling was 1419 lb-in. This relatively large value resulted in exhaust end overhang dominated second and third modes, with the second falling inside the operating speed range and the third just above maximum operating speed. The steam end journal was straddled by a double collar self-equalizing tilting pad thrust bearing of 37.8 in^2 area per side.

Tilting Pad Bearings and Coupling Retrofit

A coupling change was made in 1990 replacing the original gear design with a dry disc style. Unfortunately, however, the effective overhung moment was only slightly reduced by 8.3 percent to 1302 lb-in. Consequently, there was no noticeable change in the locations of the first three critical speeds or associated amplification factors. Essentially, all that had been eliminated were the lubrication and maintenance requirements of the gear coupling.

The sleeve bearings were retrofitted with tilting pad designs in 1993 comprising a five pad load-between-pivot configuration. The pad axial lengths were reduced to 3.0 inch at the steam end and 3.375 inch at the exhaust end, yielding slightly increased unit loads of 158 and 191 psi, respectively. Even though the tilting pad bearings had some axial misalignment capability, they were designed to fit the original bearing case spherical seat to minimize rework of field components. As with the coupling change, this retrofit hardly altered the rotor's overall transient response characteristics due to only a small reduction in the average direct bearing stiffness of 1,800,000 lb/in, with rubs still experienced during startups.

An increase in tilting pad axial length ideally should have been made to decrease the bearing unit loading thereby yielding a softer hydrodynamic oil film. This would have decreased the bearing stiffness, thus increasing the effective bearing damping as reported in Nicholas and Kirk (1982). However, dimensional constraints of

the original housings limited the axial length of the tilting pad retrofits that could be accommodated.

ROTOR-BEARING UPGRADE

As part of a review of the possible causes of the startup rub problems, the dynamic characteristics of the rotor, particularly the sensitivity of the first critical speed, were brought into question. Other areas of concern were the location of the second critical speed falling in the normal operating range, as well as the close proximity of the third to the maximum operating speed. Hard rubs were often observed between the wheels in the double flow section (Figure 9), which is an area of high response in a second mode unbalanced condition. In order to improve the stiffness flexibility ratio and hence better balance the rotordynamic system, one of the solutions proposed was to add a squeeze film damper in an attempt to reduce the sensitivity of the first critical speed as well as lower the second below the operating range. Since it was known that the addition of a squeeze film damper would lower the third critical speed, which could not be tolerated due to its close proximity to the operating range, a coupling change and turning gear wheel modification were also made to reduce the effective overhung moment.

Coupling and Turning Gear Wheel

The relatively small shaft diameter through the exhaust end bearing and coupling area combined with the heavy weights of the coupling and turning gear wheel resulted in an exhaust end overhang dominated third mode response. Since no major changes could be made to the rotor geometry, the only practical alternatives were to lighten or make integral (for stiffness) all shrunk-on components. An integral coupling flange could not be used since the turning gear wheel had to be removable for replacement in the case of tooth damage. Reducing weight, therefore, was the only approach that could be taken.

The coupling was replaced with a reduced moment disc style having an effective overhung moment of 622 lb-in, a 48 percent reduction. The original turning gear wheel was straight-sided with an overall width of 2.5 inches. By profiling the sides (Figure 12), an additional overhung moment reduction of roughly 25 percent was also achieved. Other rotor changes involved the five shrunk-on shaft sleeves located in the high-pressure labyrinth packing area. These sleeves were changed from shrunk-on to integral. The main purpose here was to eliminate the possibility of the sleeves coming temporarily loose during thermal transients, a problem that had occurred in the past and another factor that could aggravate a rub. Although the increase in shaft stiffness as a result of this modification was negligible, it was a change in the right direction.

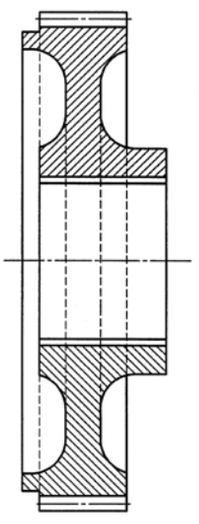

Figure 12. Profiled Turning Gear Wheel.

Squeeze Film Damper

A schematic and two photographs of the steam end squeeze film damper are shown in Figures 13 to 15, respectively. The inner bearing is a new tilting pad design comprising four pads oriented in a load-between-pivot configuration. Although the stiffness and damping characteristics of this bearing by itself are somewhat similar to the five pad design, this configuration was chosen due to symmetry considerations that help to reduce the overall response levels as documented in Nicholas and Kirk (1982).

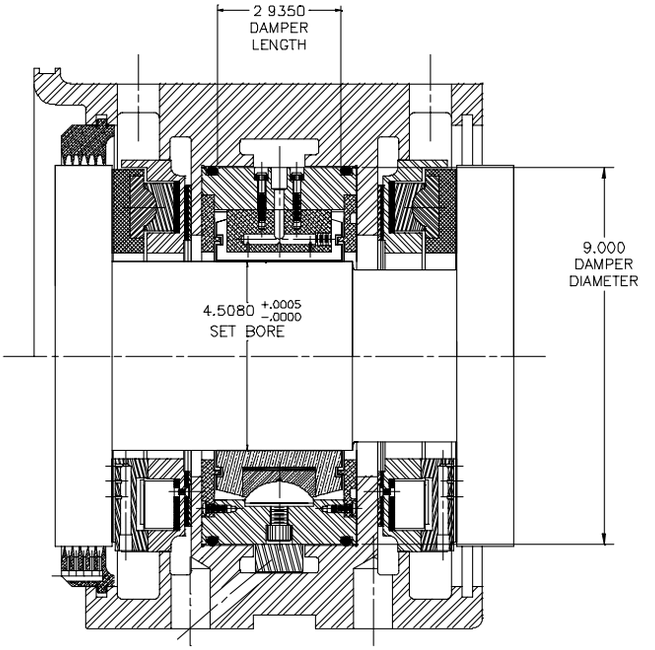

Figure 13. Schematic of Steam End Squeeze Film Damper Bearing.

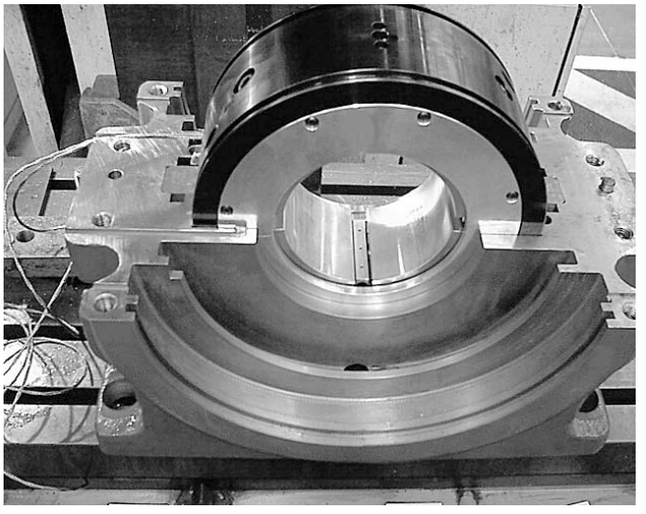

Figure 14. Steam End Housing with Journal Bearing Installed.

The inner bearing is supported and centered in the housing by an arc spring, which is bolted into the housing at the horizontal split (Figure 15). Ground shims placed at the housing shoulder underneath the arc spring seat at the bolted joint were used to facilitate centering. A small controlled radial clearance is required between the housing and inner bearing to provide the cavity for the squeeze film damping action. Oil is supplied to this cavity and the inner bearing via an annular groove machined into the housing. The inner bearing is free to float in this cavity, which is filled with oil

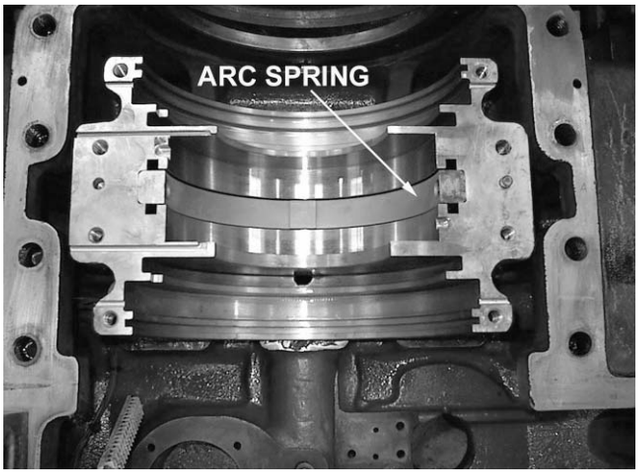

Figure 15. Steam End Housing Illustrating Arc Spring.

and enclosed by O-ring end seals. The outside diameter of the inner bearing forms the damper journal, which whirls but does not spin, thus squeezing the oil in the small annular clearance that in turn generates an oil film pressure and, subsequently, a damping force.

The theory on which the damper analysis is based is presented in Edney and Nicholas (1999). Assuming a cavitated oil film, the equations used for stiffness and damping from Gunter, et al. (1975), are:

$$K_d = \frac{2\mu R L^3 \varepsilon \omega}{c^3\left(1-\varepsilon^2\right)^2} \tag{1}$$

$$C_d = \frac{\pi \mu R L^3}{2c^3\left(1-\varepsilon^2\right)^{3/2}} \tag{2}$$

Arc Spring Design and Testing

The centering device shown in Figure 15 is an arc spring identical to that presented in Edney and Nicholas (1999). It has a semicircular profile and, at bottom dead center, the inside radius of the arc spring has a raised saddle designed for line contact with the bottom of the inner bearing housing, providing support in the vertical direction only. The arc spring is designed with a predetermined stiffness and is preloaded to offset half the rotor weight to center the inner bearing in the housing.

The arc spring analysis methodology is given in Edney and Nicholas (1999). The same design was used in both the steam and exhaust end dampers. The final dimensions were as follows: 4.570 inch inner arc radius, 5.150 inch outer arc radius, and 1.125 inch axial width for a maximum static load of 2900 lb.

The effectiveness of a damper is largely dependent on how well it is centered under load. The best means of achieving this is through static or deflection testing as described in Edney and Nicholas (1999). Test data for the steam end arc spring are plotted in Figure 16. Both sets of data are in excellent overall agreement. The average measured stiffness of 289,017 lb/in is in good agreement with the finite element prediction of 304,622 lb/in, low by only 5.1 percent. The measured deflection of 0.0108 inch at the design static load also compared well with the 0.0095 inch calculated from the finite element model. In the free condition, the vertical position of the arc springs was offset with appropriate thickness shoulder shims. This offset was verified during machine assembly, with plastigage impressions made of the damper radial clearance with the rotor installed.

ROTORDYNAMICS

The mass elastic model generated for the rotordynamics analysis is shown in Figure 17. In all the analyses conducted, a support

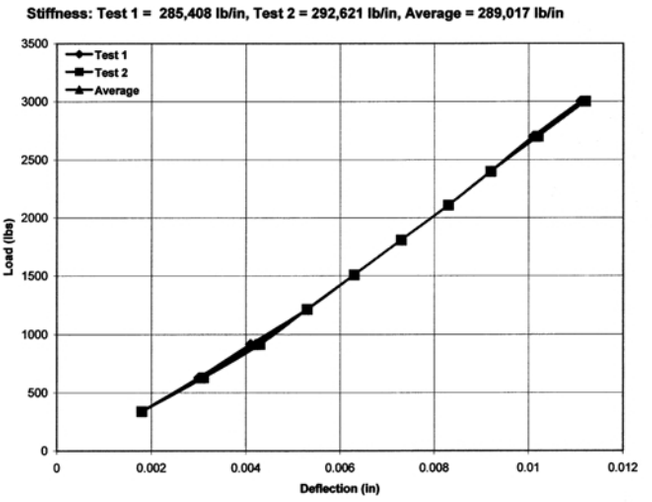

Figure 16. Load Versus Deflection Curve for Steam End Arc Spring.

stiffness and mass of 3,000,000 lb/in and 300 lb, respectively, were used at both bearings. A damping value equal to 10 percent of critical was assumed as in Nicholas, et al. (1986).

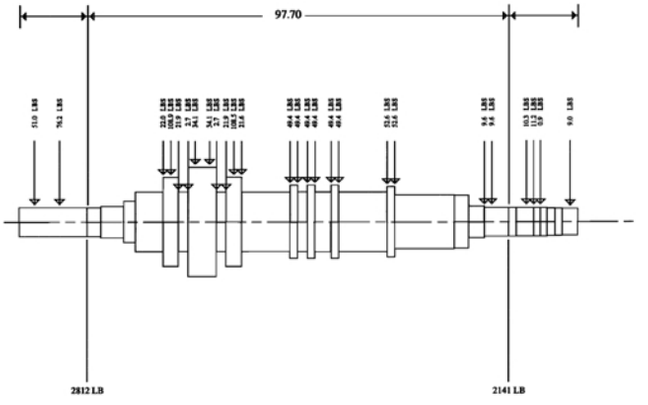

Figure 17. Mass Elastic Model of Rotor.

Undamped Critical Speed Map

An undamped critical speed map of the rotor in the original configuration is shown in Figure 18. Plotted on this map are the dynamic stiffness curves appropriate to the initial five pad tilting pad bearing retrofit. It is clearly evident from this figure that the rotor was operating in the vicinity of the second critical speed, with small margin from the third. The third mode, being the first truly flexural mode, is highly responsive and ideally should be as far above the maximum operating speed as practical. Furthermore, the free-free asymptote of this mode tends toward 8180 cpm, which is below the maximum speed of 8400 rpm. Clearly, with this rotor configuration there is little that can be done to tune the critical speeds in relation to the operating range through a bearing change alone. This condition prompted the effort to reduce the exhaust end overhung moment.

The undamped critical speed map for the new rotor configuration with the reduced exhaust end overhung moment is given in Figure 19. Plotted on this map are the dynamic stiffness curves corresponding to the new four pad tilting pad bearing combined with the squeeze film damper. The resultant stiffness of the damper bearing is 437,000 lb/in, which is much lower compared to the original sleeve and initial five pad tilting pad designs. This stiffness is roughly one-fifth of the shaft stiffness and more than adequately meets the stiffness flexibility ratio rule.

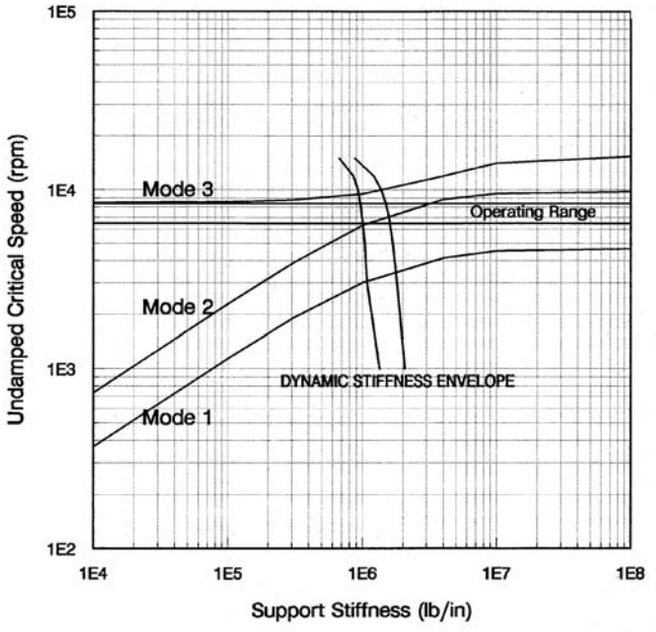

Figure 18. Undamped Critical Speed Map – Original Rotor Configuration.

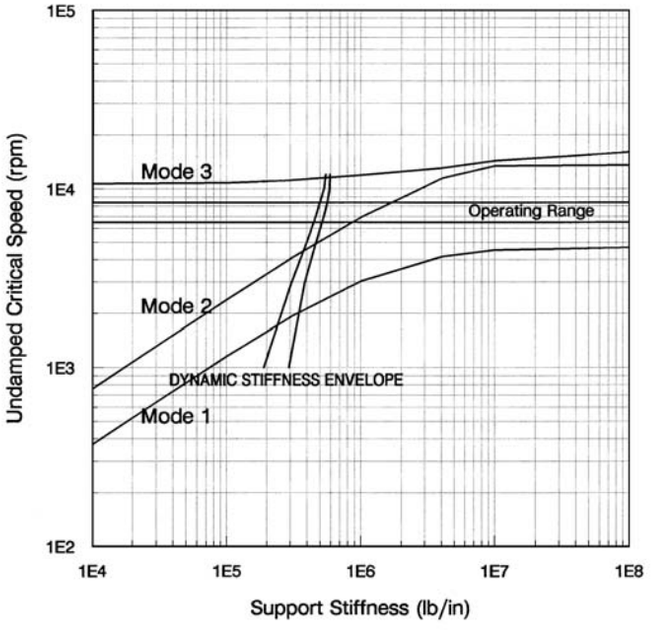

Figure 19. Undamped Critical Speed Map – Rotor with Reduced Overhung Moment.

Furthermore, with the reduced overhung moment, the third mode free-free asymptote of 10,670 cpm is now well above the maximum operating speed. Also evident from Figure 19 is that in order to reduce the second mode below the operating range, a bearing stiffness well below 800,000 lb/in is required. While this could not have been achieved with a conventional bearing (sleeve or tilting pad), this turned out to be a secondary benefit of adding the squeeze film damper.

Unbalance Response

Calculated synchronous response plots and rotor deflected shapes comparing the three rotor-bearing configurations are included in Figures 20 to 28. The plots are at the steam and exhaust end probe locations for the first three modes. The first mode was excited with an unbalance of 19.2 oz-in, or roughly 32W/N, placed at the rotor's midspan. The second mode was excited by placing one-half of this unbalance just inboard of each journal bearing 180 degrees out-of-phase, and the third mode by placing one third at the midspan and each shaft end 180 degrees out-of-phase with the midspan.

Values for critical speed, amplification factor, and maximum amplitude at the probes are summarized in Table 1. With the squeeze film damper, the first mode amplification factors and maximum amplitudes are lower by factors of at least three.

Table 1. Comparison of Predicted Peak Response Speed (NC), Amplification Factor (AF), and Maximum Amplitude (A_{MAX}) at Probe Locations – Sleeve, Initial Five Pad Tilting Pad, and Squeeze Film Damper Designs.

Mode	NC (rpm) / AF (dim) / A_{MAX} (mils p-p)		
	Original Sleeve Bearing	Initial Five Pad Tilting Pad Retrofit	Squeeze Film Damper
First	3,800 / 5.1 / 2.20	3,500 / 5.8 / 3.05	2,000 / 1.9 / 1.55
Second	7,500 / 3.1 / 2.40	7,000 / 4.6 / 3.00	4,900 / 1.3 / 2.65
Third	9,600 / 6.4 / 17.5	9,600 / 9.6 / 18.5	11,350 / 11.4 / 27.5

Figures 20 and 21 illustrate the response plots for a first mode unbalanced condition, and Figure 22 the deflected mode shapes at the respective peak response speeds. With the squeeze film damper, the first peak response speed is critically damped. The maximum amplitude at the probes is lower by at least 25 percent compared with the original sleeve and initial five pad tilting pad bearings.

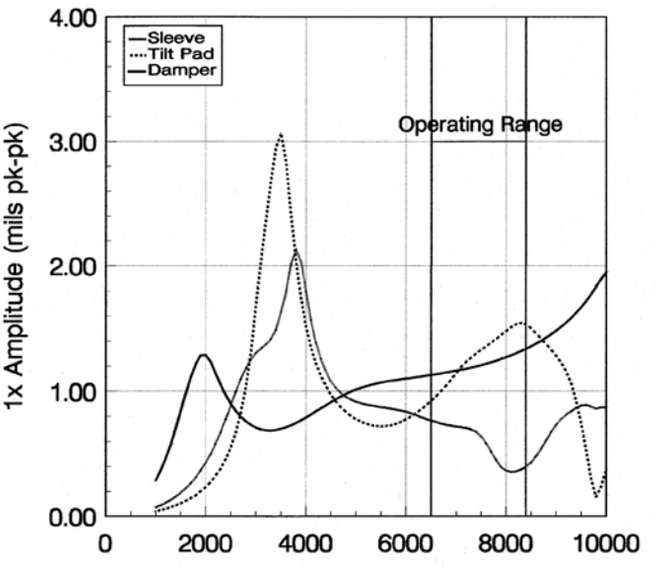

Figure 20. Steam End Probe Response – First Mode Excitation.

Of more interest, however, is the rotor's general shape and reduction in midspan amplitude as shown in the deflected shape plot of Figure 22. The rotor's deflected shape with the damper bearing is almost purely straight, with a reduction in midspan amplitude of greater than 50 percent. In this condition, the possibility of an interstage rub is greatly reduced.

This plot also helps in explaining the difficulty of controlling the rotor's vibration with the conventional bearings. The locations of the nodal points are determined by the relative flexibility of the rotor compared with the resultant support flexibility, with two consequences as the nodal points move closer to the bearings. First, the effective bearing damping is greatly reduced due to the restricted motion in the bearings. Second, the response amplitude at the rotor's midspan is considerably greater than at the probe locations. This latter situation can lead to a potentially damaging

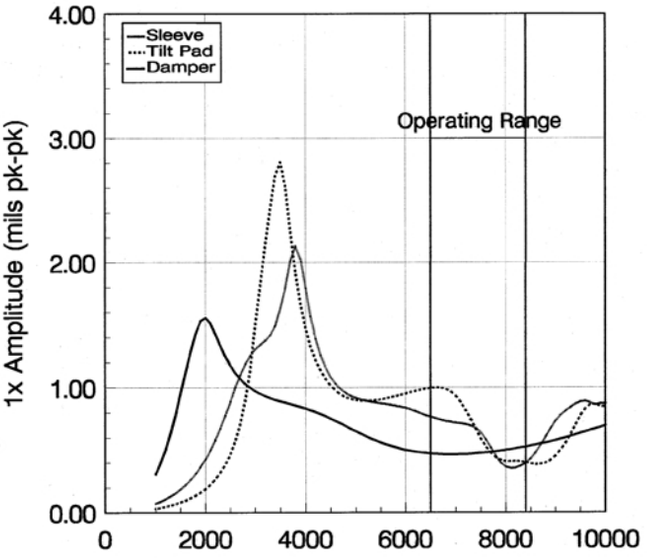

Figure 21. Exhaust End Probe Response – First Mode Excitation.

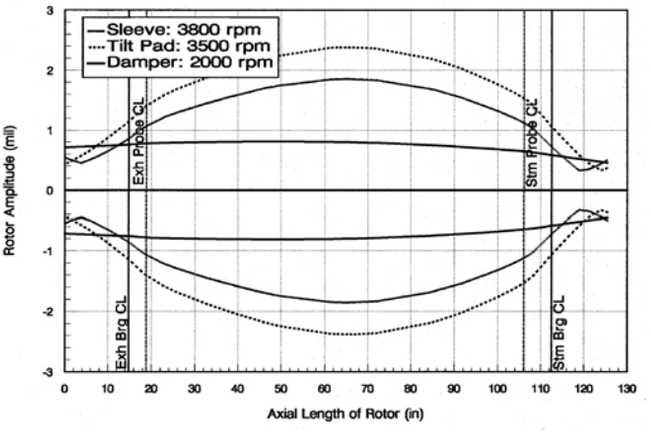

Figure 22. Rotor Deflected Shape at Peak Response Speed – First Mode Excitation.

rub condition if the midspan vibration amplitude builds up sufficiently to exceed the running clearances at the interstage seals. With the squeeze film damper, however, the nodal points are now sufficiently away from the bearings with enough relative amplitude to allow the available bearing damping to be more effective.

The second mode response plots are included in Figures 23 and 24, and the deflected shape at the respective peak response speeds in Figure 25. With the squeeze film damper, the second peak response is critically damped and well below the minimum operating speed. Although the response over the operating range at the probe locations indicates only a slight improvement, the deflected shape plot illustrates the primary benefit. With the damper, the new coupling, and the new turning gear wheel, the exhaust end overhung response is almost entirely eliminated with a reduction in shaft end amplitude by a factor of three. Furthermore, this mode is quickly passed through as the turbine is brought up to speed. With the conventional bearings, this mode was in the vicinity of the normal operating range and could be excited by any residual unbalance in the rotor assembly. A common source of overhung unbalance is from the coupling, which would greatly aggravate the overhung response of this mode. With the conventional bearings, heavy rub marks were often observed in the double flow section of the rotor, which could be indicative of this overhung mode being excited possibly from residual unbalance in either the coupling or coupling fit.

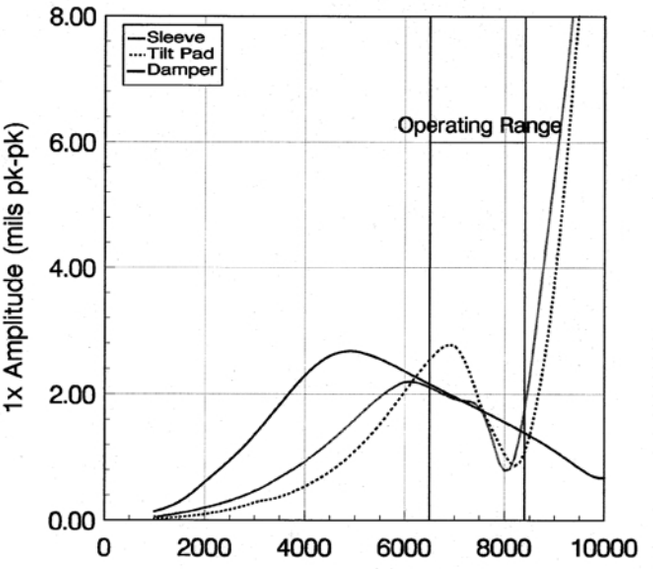

Figure 23. Steam End Probe Response – Second Mode Excitation.

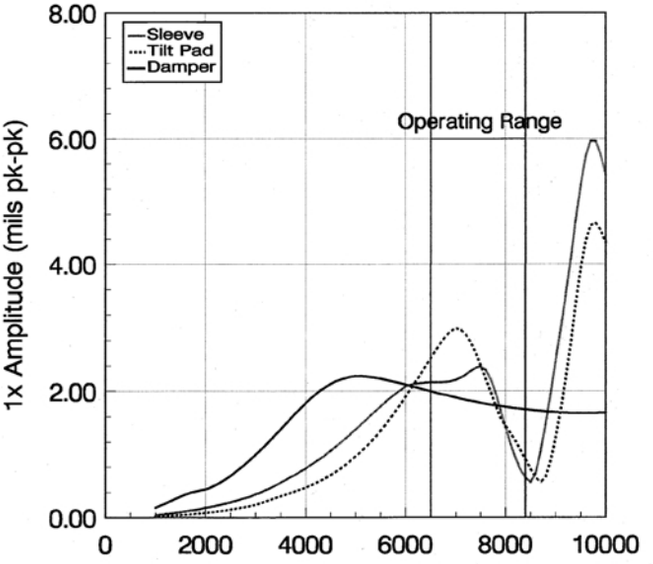

Figure 24. Exhaust End Probe Response – Second Mode Excitation.

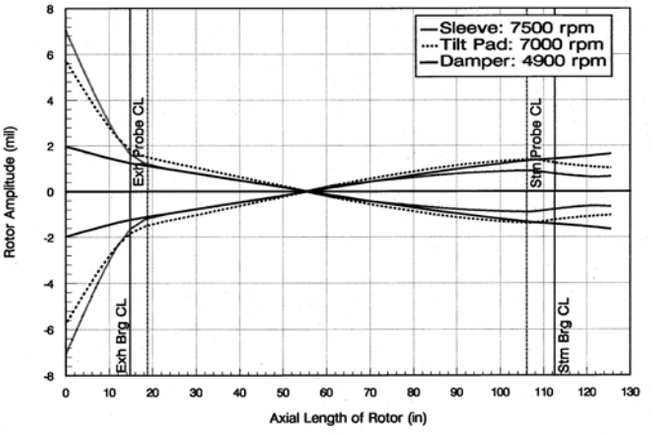

Figure 25. Rotor Deflected Shape at Peak Response Speed – Second Mode Excitation.

The third mode response plots of Figures 26 and 27 best illustrate the improvement with the reduced exhaust end overhung moment. The third critical speed is raised almost 2000 rpm and is well above the maximum operating speed. The response at the probe locations over the normal operating range are also lower, by a factor of two at the low end of the speed range and six at the high end.

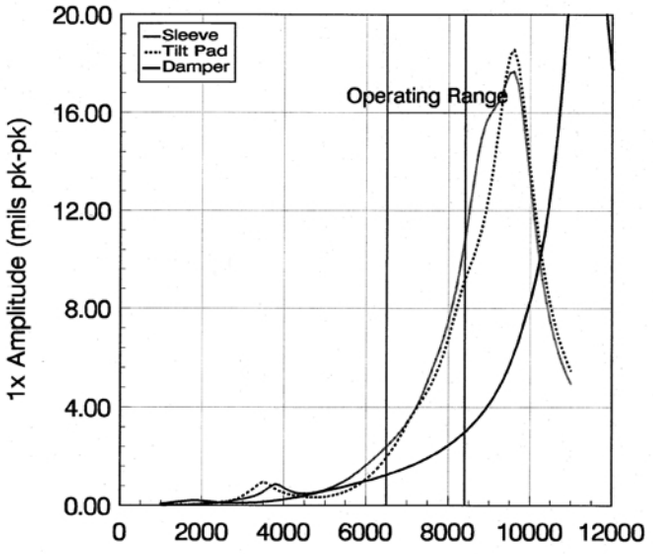

Figure 26. Steam End Probe Response – Third Mode Excitation.

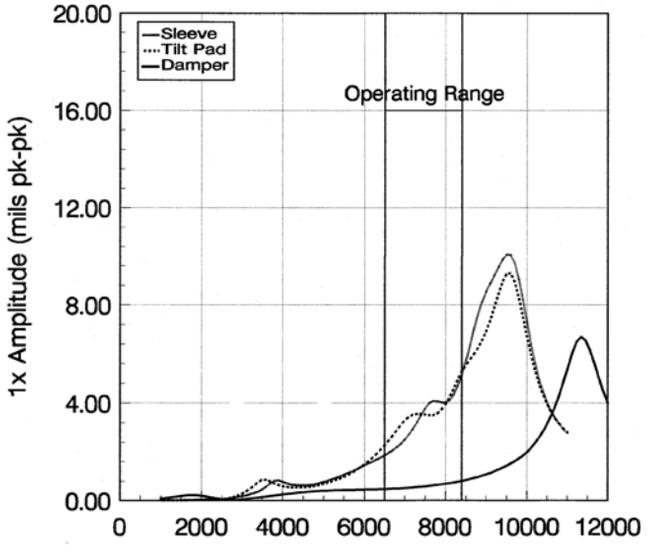

Figure 27. Exhaust End Probe Response – Third Mode Excitation.

The overhung influence is best illustrated in the deflected shape plot given in Figure 28. In this figure, the deflected shapes are all at the maximum operating speed of 8400 rpm, and not their respective peak response speeds. In the new configuration the maximum response, which is at the exhaust end, is lower by roughly a factor of two. Clearly, the reduced overhung moment resulting from the coupling change and turning gear wheel modification were necessary in successfully tuning the rotor's dynamic characteristics in relation to the operating speed range.

Stability

The initial results of an eigenvalue stability analysis of the original sleeve, five pad tilting pad, and squeeze film damper designs are compared in Table 2 at the maximum operating speed of 8400 rpm. The values given for damped natural frequency and

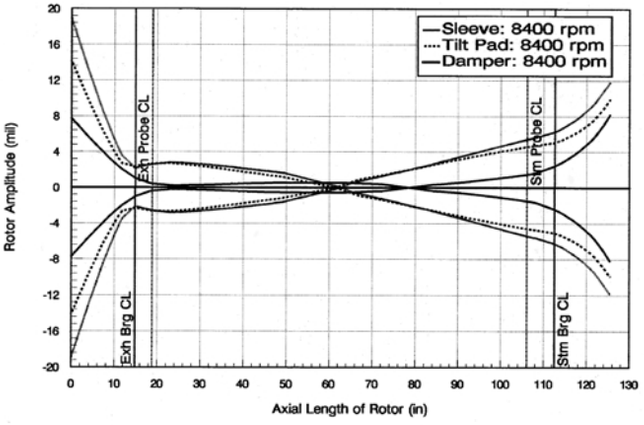

Figure 28. Rotor Deflected Shape at 8400 rpm – Third Mode Excitation.

logarithmicdecrement correspond to the first forward whirl mode. With the squeeze film damper, the dynamic stability is improved by a factor of two over the initial five pad tilting pad design. In the original configuration with pressure dam bearings, the system was marginally stable although there were no reported instability problems.

Table 2. Comparison of Eigenvalue Analysis at 8400 rpm – Sleeve, Initial Five Pad Tilting Pad, and Squeeze Film Damper Designs.

Bearing Design	Damped Natural Frequency (rpm)	Logarithmic Decrement (dim)
Original Sleeve	3,639	-0.03
Initial Five Pad Tilting Pad Retrofit	3,289	0.34
Squeeze Film Damper	1,949	0.67

TURBINE CASING HORIZONTAL JOINT STEAM LEAK

Possible causes of a casing joint steam leak include repeated startups, improper makeup, damaged joint faces, warped joints, and incorrect design. Of these, startup is by far the most critical and has the greatest potential for resulting in permanent damage. During startup, the casing inside diameter (ID) heats up at a faster rate than the outside diameter (OD), creating a thermal gradient across the casing wall. This thermal gradient tries to make the ID expand, which is constrained by the OD. If the gradient is large enough, the ID and/or flange faces will yield and permanently deform. Once steady-state conditions are reached and the gradient has reduced, the yielded area inside of the bolt pattern will open up providing a pocket for steam erosion or wire drawing. This condition can be avoided by not starting up a machine too quickly, thus minimizing these harmful thermal gradients.

Repeated thermal cycling can aggravate this condition compounding the residual stresses and hence casing distortion. As the stress levels rise, the yielding increases causing the casings to distort further out-of-round. In some instances, the horizontal joint will also warp, further opening up gaps. Improper makeup, on the other hand, is the most common reason for leakage usually through not following the correct assembly procedure and/or stud-tightening diagram and values. Less common reasons include incorrect flange design and damaged faces by not protecting them when the casing is open.

Over the years, the subject machine had quite a history of horizontal joint leak problems. In addition to the performance, integrity, and safety concerns, it was thought that these leaks could have been contributing to the rub problems through casing distortion from thermal differentials affecting the internal alignment. On initial disassembly of the machine, the sealing surface of the

horizontal joint was found to be in somewhat poor condition. Given the short duration of the turnaround, however, no time was available in the schedule to remachine the split (and hence casing bore) to fully restore the sealing faces. After further evaluation, it was decided that the sealing surface was probably in good enough condition to provide a seal and no corrective action was taken.

A prior review of the horizontal joint design concluded that it was not optimal. In the high-pressure section, for example, the sealing area was quite large contributing to a low overall contact pressure. The modified design is illustrated in Figure 29, with a photograph of the remachined face shown in Figure 30. The crosshatched portion clearly shows the extent of the relieved area to provide a more uniform and increased contact pressure in the high-pressure section. A small portion of the face, as indicated by the solid shaded region, was built up with weld to prevent a leakage path across the horizontal joint. In addition to this remachining, a revised stud-tightening diagram was issued with slightly increased torque values.

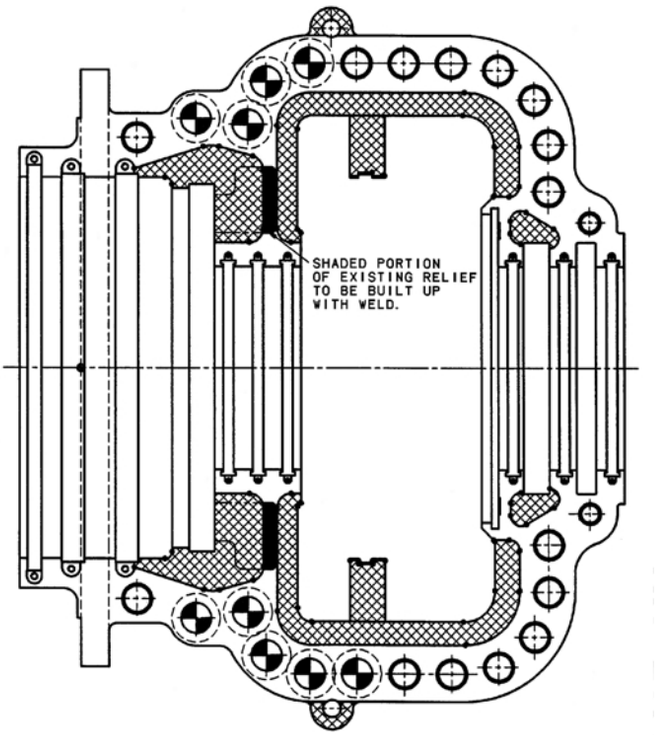

Figure 29. Horizontal Joint Modification.

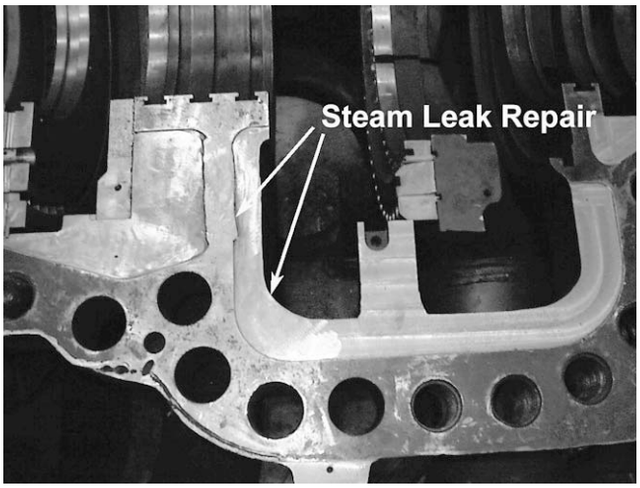

Figure 30. Remachined Horizontal Joint.

During torquing of the horizontal joint, however, space constraints prohibited the use of power driven torquing equipment in the transition region between the high-pressure casing and barrel section. Consequently, the studs in this area were tightened manually using a wrench and hammer. The reworked horizontal joint initially performed satisfactorily with no steam leakage. After roughly six months of operation, however, a small steam leak appeared in approximately the same region as before, where the studs had been manually torqued. Manually retightening the studs helped to reduce the leak.

TURBINE CASING REFURBISHMENT

The steam turbine case is designed to be free-floating. Keys and keyways allow movement in the horizontal, vertical, and axial directions for casing thermal expansion. After years of operation, the keys were found to be bound in the keyways, thus preventing the case from growing uniformly and hence contributing to a rotor-casing rub condition.

A bound exhaust end horizontal key is shown in Figure 31. With the exhaust end foot removed, the key and keyway were cleaned (Figure 32), lubricated, and reassembled. The exhaust end bearing case bracket axial, horizontal, and vertical keys and/or keyways are shown in Figure 33 after disassembly and cleaning. The horizontal and vertical keys are combined as one set of "T" shaped keys on either side of the main turbine case. The exhaust end bearing case is free-floating, and is fitted to the bearing case bracket by sliding over the top of the vertical protrusions of the "T" keys and down into the axial keyway. All keys and keyways were lubricated prior to reassembly.

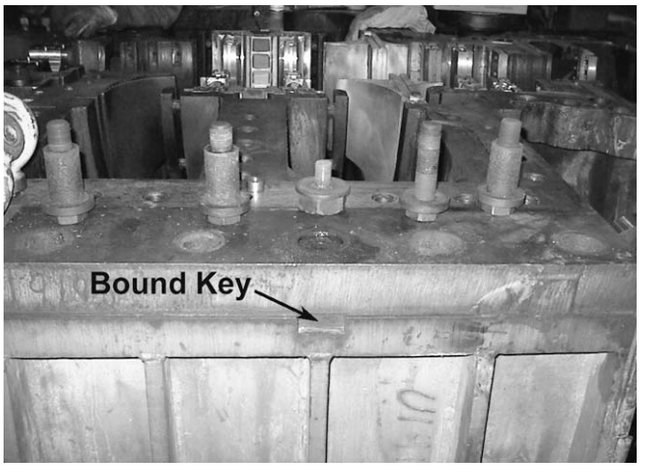

Figure 31. Bound Lateral Expansion Key in Exhaust End Casing.

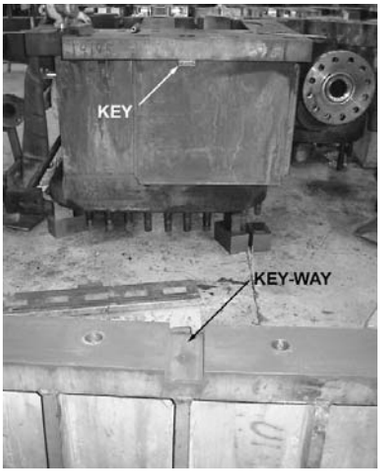

Figure 32. Cleaned Keyway in Exhaust End Casing.

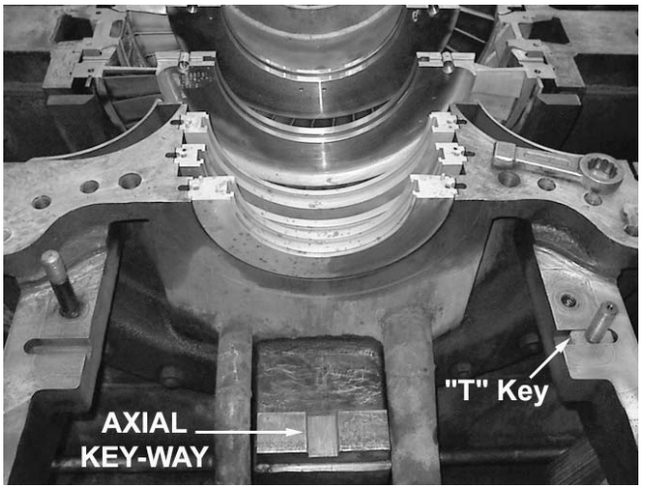

Figure 33. Exhaust End Bearing Case Bracket after Cleaning.

FOUNDATION REPAIR

A deteriorated support was another possible contributor to the turbine's high vibration problems. The foundation was examined and some cracks were discovered in the concrete beams supporting the baseplate. Additionally, poor grout placement and degradation caused by oil and steam leakage over the years resulted in large gaps at the interface of the baseplate and concrete foundation. The overall poor condition of the concrete foundation and grout interface had the effect of increasing the foundation flexibility, thereby reducing the bearing's effective damping and increasing rotor vibration (Nicholas, et al., 1986).

Clearly, a foundation repair was necessary. While the rotor and turbine case were undergoing rework and repair, the 9500 lb baseplate was removed from its concrete pad (Figures 34 and 35). In order to ensure the correct position of the baseplate during reinstallation, optical references were taken by attaching reference plates to the bottom of the concrete foundation using drop-in anchors. In addition, leveling references were taken by means of a precision site level.

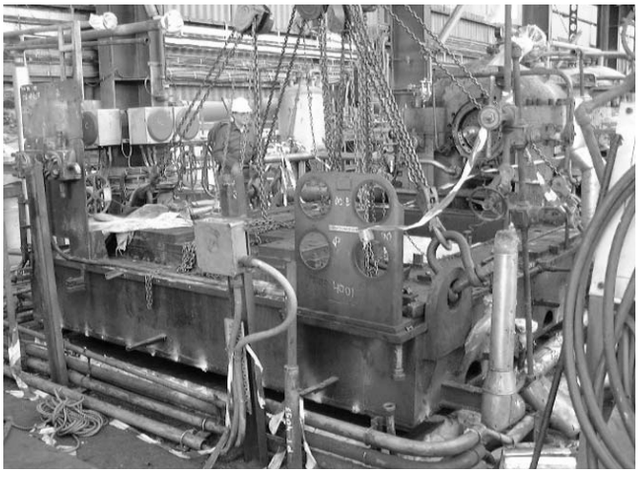

Figure 34. Baseplate Lifted from Foundation.

From Figure 36, the deterioration of the grout under the removed baseplate is evident. Furthermore, after a careful inspection, many cracks were observed in the concrete beams emanating from the anchoring bolts. The whole area was cleaned and sandblasted. A repair was made that comprised injecting the cracks with a pressure epoxy adhesive as shown in Figure 37.

Figure 35. Baseplate Removed from Foundation.

Figure 36. As-Found Deteriorated Condition of Foundation.

Figure 37. Foundation after Repair.

The anchoring bolts were inspected for cracks to assure their integrity and the mounting pads rebuilt using an epoxy resin (Figure 37). The baseplate was also cleaned, sandblasted, and repainted.

Four days before the steam turbine arrived back on site, the baseplate was reinstalled. Its position and level were accurately set in accordance with the recorded references. After the baseplate bolts were tightened, grout forms for the outboard and inboard ends were installed.

Once the turbine arrived on site, it was reinstalled onto the baseplate, the internal rotor-to-casing alignment checked, and an initial alignment to the first body ethylene compressor made. The baseplate was then grouted using an epoxy resin and left to cure for a period of 24 hours. While the grout cured, no major weights were added or removed from the baseplate. Once the epoxy was set, the turbine case upper half was reinstalled, the turbine-to-compressor final alignment was made, and the steam piping connected.

RETRACTABLE PACKING RETROFIT

Another potential problem area concerned the shaft labyrinth packing. As discussed, this steam turbine experienced numerous rotor and packing rubs while passing through the first critical speed causing excessive vibration and shutdowns (Figures 9 and 10). A recent paper entitled "Steam Turbine Risk Assessment" (Christ, et al., 1997) stated that for steam turbines, "The highest risk component is rubs of labyrinth seals that occur during test and startup." In addition to high vibration, rubs bring about wear and increased leakage of the seals that degrade turbine efficiency, thus limiting plant production. For this reason, rubs, and hence premature wear of the labyrinth seals, should be avoided if at all possible.

One source of steam turbine packing rubs is thermal gradients. Unequal heating prior to and during startup can distort any shaft sleeves attached to the rotor under the labyrinth seal. This distortion reduces the packing clearance causing a rub. This situation is aggravated when passing through a responsive first critical speed as was the case with this turbine (Figures 2 to 6). Even without thermal gradients, traversing a responsive critical speed can often result in a severe rub.

Localized heating during startup as a result of packing rubs due to thermal gradients and/or passing through responsive critical speeds will cause a turbine rotor to bow. This is a cumulative condition since the rub generates heat at the rotor's high spot, which in turn causes both the rotor and stationary parts to expand rapidly. The induced thermal bow introduces unbalance, which results in an even harder rub.

Another source of rubs is from starting the turbine with a bowed rotor. If after a turbine is shutdown and the rotor is allowed to come to rest, the upper side of the rotor will become hotter than the lower side due to hot vapor in the turbine case accumulating in the upper half. This temperature differential around the shaft will cause the rotor to take a bow, which will remain until the temperature is equalized. The extent of the bow is dependent on the differential temperature, and size and length of the rotor. To avoid this condition, the rotor should be slowly rotated with a turning gear, allowing the shaft temperature to equalize. Admitting steam to a stationary turbine or improper use of sealing steam can also cause temporary rotor bows. Starting a turbine with a bowed rotor will almost always lead to a rub.

In order to address some of these packing rub concerns, most steam turbine manufacturers utilize packing rings with springs designed to force the packing ring segments toward the shaft into a tight clearance position. A typical conventional labyrinth packing ring design is shown in Figure 38 (Johns, et al., 1997). Each segment is typically held in place by a flat spring located behind the packing. The spring holds the segment at its minimum clearance position during assembly and startup. A typical diametral clearance between the rotating shaft and stationary packing is of the order 20 to 25 mils.

As steam pressure builds up on the upstream side of the packing, the packing segment moves downstream against a hooked shoulder fit forming a seal. The force holding the packing ring radially toward the shaft is a combination of the spring force and the force

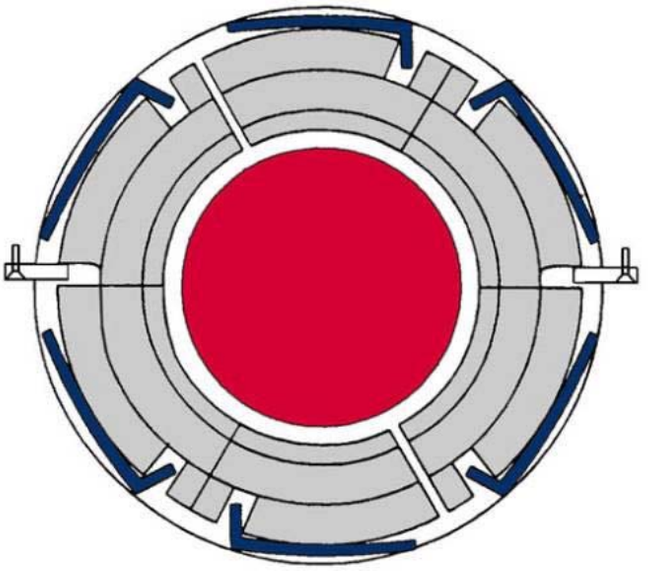

Figure 38. Conventional Labyrinth Seal Ring.

of the steam acting on the backside of the packing ring. As the steam flow increases, the ability of the packing segment to move away from the shaft is significantly reduced. Under this condition, the shaft packing becomes essentially rigid. In theory, any rubbing that might occur should happen during runup through the first critical speed at relatively low steam flows and, thus, low steam forces. This would allow the packing segment to be pushed away from the shaft minimizing rub damage and rub-induced vibrations.

An alternate approach would be to somehow keep the packing clearances wide open during the startup and shutdown period when rubs normally occur, and tight during normal load and full speed operation. Retractable packing (Johns, et al., 1997) operates in this fashion. In the standard packing described above, the spring pressure holds the packing toward the turbine shaft, and as the turbine load increases, the steam pressure adds force behind the packing, keeping the seal clearance tight. With retractable packing, the springs hold the packing away from the shaft as in Figure 39, and as the turbine load increases, the steam pressure behind the packing forces the packing toward the shaft into the tight clearance condition (Figure 40).

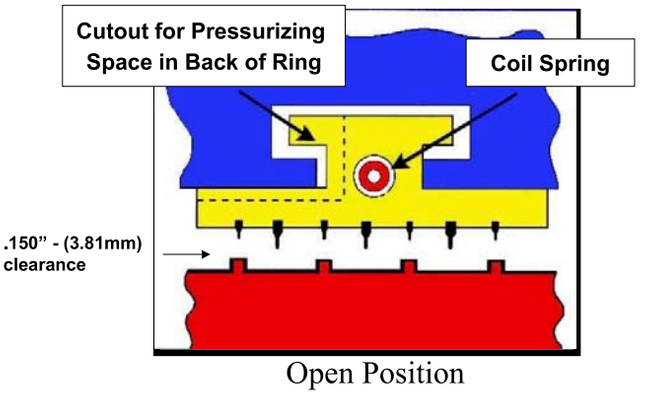

Figure 39. Cross Sectional View of Retractable Seal in Open Position During Startup.

By proper design of the coil springs between packing segments, the pressure forces acting on the packing can be utilized to cause the packing to move from a large clearance to a small clearance at a predetermined flow. The packing is designed to close beyond the point where thermal gradients occur and above the critical speed range. Figure 41 shows the typical difference in clearances for

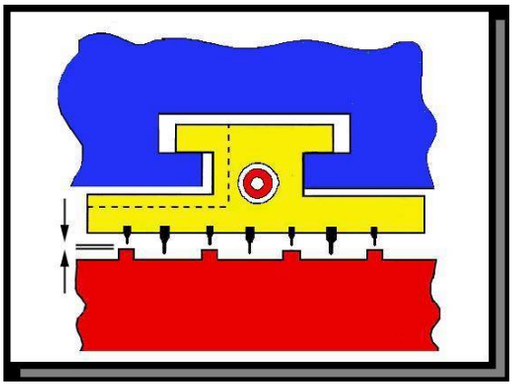

Figure 40. Cross Sectional View of Retractable Seal in Closed Position for Operation.

conventional packing and retractable packing during startup when the rotor vibration increases while passing through the first critical speed.

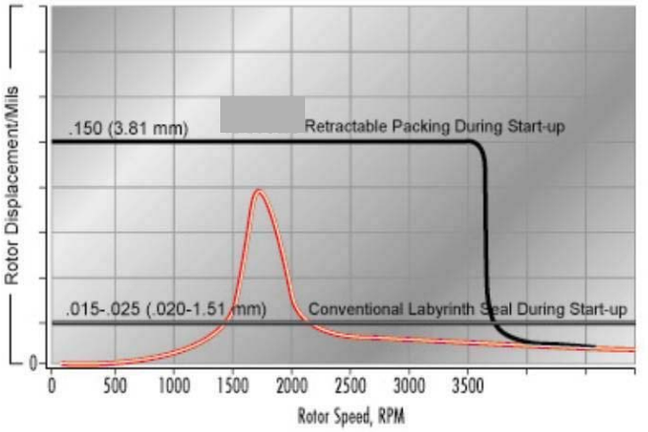

Figure 41. Rotor Vibration Characteristic During Startup.

No major rework to the turbine was required to fit the retractable packing with only minor modification to the packing grooves in the diaphragms. Eight rows of retractable packing were retrofitted into the turbine. They were located in the high-pressure end nozzle and diaphragm stages up to the exhaust section. An example is shown in Figure 42.

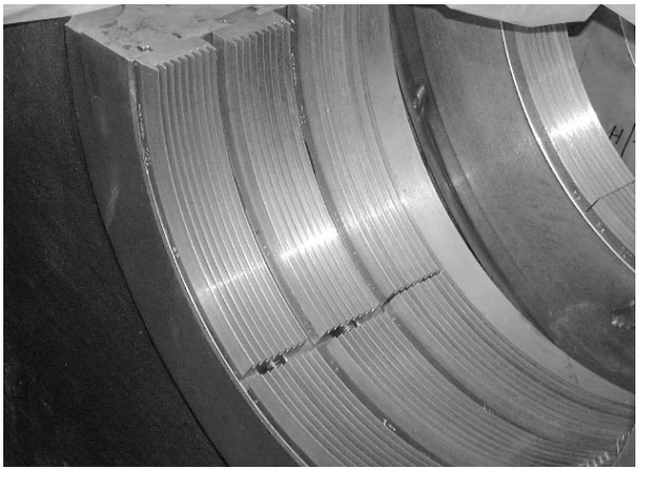

Figure 42. Retractable Seals Installed in High-Pressure Packing Case.

FIELD STARTUP

Forty-six days after shutdown, the turbine was ready for overspeed testing in July 2000. After setting the mechanical trip, the turbine was coupled to the ethylene compressors and the train made ready for plant startup.

After a first startup, the unit was shutdown due to a process-related problem. On August 1, 2000, the unit was restarted and the train speed increased to 7200 rpm. No rubs or vibration related problems were detected either going through the turbine rotor's first critical speed or in the operating speed range. The turbine exhibited the lowest rotor and casing vibration amplitudes ever recorded. Figure 43 shows 1× levels below 10 microns peak-to-peak (0.4 mils peak-to-peak).

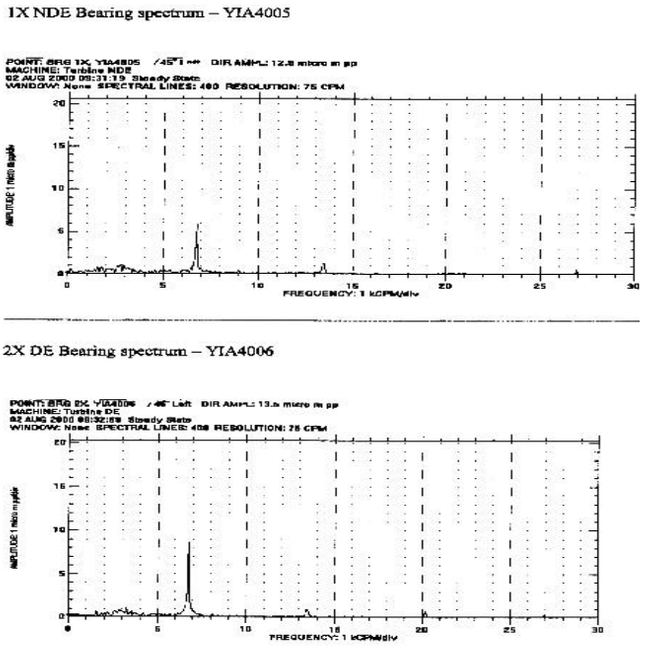

Figure 43. Operating Speed Vibration Spectra After Overhaul.

A time history of turbine vibration from September 2000 until January 2001 may be seen in Figures 44 and 45. From Figure 44, the steam end horizontal displacement probe's normal vibration levels are around 20 microns peak-to-peak (0.8 mils peak-to-peak). This is half the value from Figure 7 before the overhaul. There are a handful of vibration excursions that remained under 50 microns peak-to-peak (2.0 mils peak-to-peak) in Figure 44 compared to peaks ranging up to 125 microns peak-to-peak (4.9 mils peak-to-peak) from Figure 7.

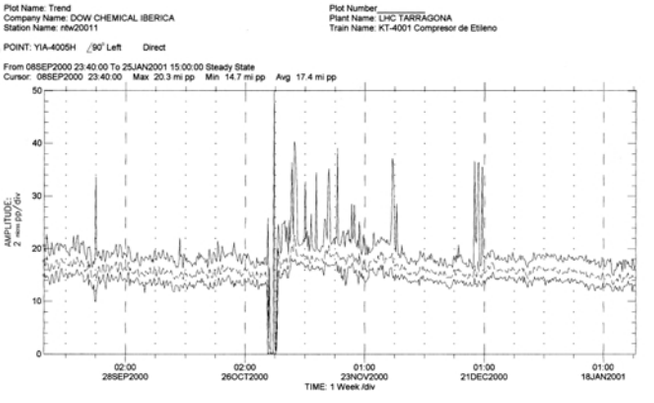

Figure 44. Time Trend of Steam End Horizontal Displacement Probe Vibration After Overhaul.

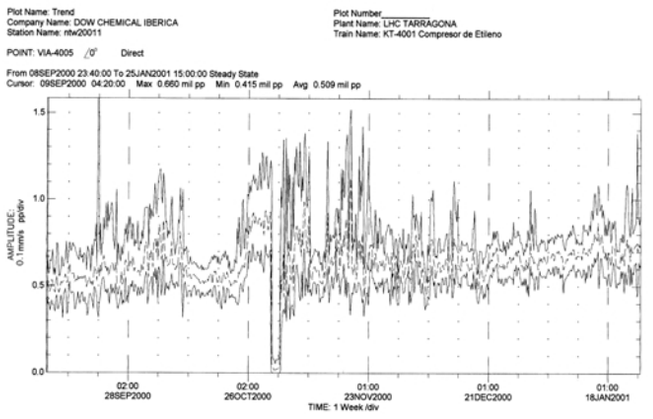

Figure 45. Time Trend of Exhaust End Horizontal Bearing Case Velocity Probe Vibration After Overhaul.

Casing readings for the exhaust end horizontal velocity probe (Figure 45) all range below 1.6 mm/s zero-to-peak (0.06 in/s zero-to-peak) compared to 20 mm/s zero-to-peak (0.8 in/s zero-to-peak) from Figure 8 before the overhaul. Nominal velocity levels of about 0.8 mm/s zero-to-peak (0.03 in/s zero-to-peak) are evident from Figure 45 compared to between 4.0 and 8.0 mm/s zero-to-peak (0.16 and 0.32 in/s zero-to-peak) from Figure 8.

CONCLUSIONS

- The critical speed and stability characteristics of machines with sensitive or problem rotors can be greatly improved by modifying the bearings to incorporate a squeeze film damper. If performed carefully, this solution can be implemented relatively quickly and inexpensively compared to other options such as modifying the rotor and/or the case.

- The dynamic stability of a rotor supported on conventional bearings (either sleeve or tilting pad) can be significantly extended by the addition of a squeeze film damper. With the squeeze film damper, the stability threshold was increased by a factor of two compared to the initial five pad tilting pad design.

- The squeeze film damper reduced both the location and response sensitivity of the first and second peak response speeds, with both modes critically damped. The coupling change and turning gear wheel modification raised the location of the third mode and greatly reduced the sensitivity of the exhaust shaft end to coupling unbalance.

- The retractable packing retrofit contributed to both trouble-free startups and increased efficiency of the steam turbine. By eliminating normal labyrinth packing wear from rubs with the seals open during startup, tight operating seal clearances were maintained, thus reducing interstage leakage.

- Deteriorated foundations will greatly aggravate turbomachinery related vibration problems. Oil and steam leakage over the years will degrade grout, rendering the bond between the foundation and baseplate ineffective. Structurally weak foundations and supports are poor for controlling rotor vibration by reducing the effectiveness of the available damping at journal bearings.

- Effective repairs can be made to deteriorated foundations to restore them like new as described herein. Repairs of this nature must be completed with the equipment removed from the foundation to ensure no baseplate distortion.

- As part of routine maintenance, all keys and keyways should be cleaned and lubricated to ensure that they function correctly. Bound or restricted keys are a prime contributor to casing distortion that often leads to rotor-casing internal misalignment and hence rubs.

- The rub-induced startup vibration problem was successfully eliminated. The turbine is currently operating with the lowest rotor and casing vibration amplitudes ever recorded.

NOMENCLATURE

A_{MAX} = Maximum amplitude (mils)
AF = Amplification factor at NC (dim)
c = Damper radial clearance (in)
C_d = Squeeze film direct damping (lb-sec/in)
D_s = Rotor mid-shaft diameter (in)
K_d = Squeeze film direct stiffness (lb/in)
L = Damper axial length (in)
L_b = Rotor bearing span (in)
N = Maximum operating speed (rpm)
NC = Critical speed (rpm)
R = Damper radius (in)
W = Rotor weight (lb)
ε = Damper eccentricity ratio (dim)
μ = Oil viscosity (lb-sec/in^2)
ω = Shaft speed (rad/sec)

REFERENCES

Christ, T. J., Drosjack, M. J., and Tanner, G. M., 1997, "Steam Turbine Risk Assessment—A Tool to Assist in Optimizing Inspection and Overhauls of Industrial Steam Turbines," *Proceedings of the Twenty-Sixth Turbomachinery Symposium*, Turbomachinery Laboratory, Texas A&M University, College Station, Texas, pp. 87-93.

Edney, S. L. and Nicholas, J. C., 1999, "Retrofitting a Large Steam Turbine with a Mechanically Centered Squeeze Film Damper," *Proceedings of the Twenty-Eighth Turbomachinery Symposium*, Turbomachinery Laboratory, Texas A&M University, College Station, Texas, pp. 29-40.

Gunter, E. J. Jr., Barrett, L. E., and Allaire, P. E., 1975, "Design and Application of Squeeze Film Dampers for Turbomachinery Stabilization," *Proceedings of the Fourth Turbomachinery Symposium*, Turbomachinery Laboratory, Texas A&M University, College Station, Texas, pp. 127-141.

Johns, D. A., Rasmussen, D., and Beverly, J., 1997, "Turbine Remanufacture—One Option for Reliability and Efficiency Improvement," *Proceedings of the Twenty-Sixth Turbomachinery Symposium*, Turbomachinery Laboratory, Texas A&M University, College Station, Texas, pp. 95-110.

Nicholas, J. C., 1994, "Tilting Pad Bearing Design," *Proceedings of the Twenty-Third Turbomachinery Symposium*, Turbomachinery Laboratory, Texas A&M University, College Station, Texas, pp. 179-194.

Nicholas, J. C. and Kirk, R. G., 1982, "Four Pad Tilting Pad Bearing Design and Application for Multi-Stage Axial Compressors," ASME Journal of Lubrication Technology, *104*, (4), pp. 523-532.

Nicholas, J. C., Whalen, J. K., and Franklin, S. D., 1986, "Improving Critical Speed Calculations Using Flexible Bearing Support FRF Compliance Data," *Proceedings of the Fifteenth Turbomachinery Symposium*, Turbomachinery Laboratory, Texas A&M University, College Station, Texas, pp. 69-78.